The optimal density of cellular solids in axial tension

L. Angela Mihai* Khulud Alayyash* Hayley Wyatt*

Abstract

For cellular bodies with uniform cell size, wall thickness, and shape, an important question is whether the same volume of material has the same effect when arranged as many small cells or as fewer large cells. To answer this question, for finite element models of periodic structures of Mooney-type material with different structural geometry and subject to large strain deformations, we identify a nonlinear elastic modulus as the ratio between the mean effective stress and the mean effective strain in the solid cell walls, and show that this modulus increases when the thickness of the walls increases, as well as when the number of cells increases while the volume of solid material remains fixed. Since, under the specified conditions, this nonlinear elastic modulus increases also as the corresponding mean stress increases, either the mean modulus or the mean stress can be employed as indicator when the optimum wall thickness or number of cells is sought.

Keywords: cellular solids; nonlinear hyperelastic material; large strain deformation; micro-structural behaviour; material density; optimisation.

1 Introduction

In natural structures, the mechanical support system is usually formed through a combination of increase in the cell number or size and sustained sclerification (thickening and lignification) of the cell walls. Dicotyledon stems (*e.g.* magnolia, maple, oak, rose, sycamore, willow) increase their diameter primarily by cell division which ultimately form the characteristic annual rings. Monocotyledon stems (*e.g.* bamboo, corn, lily, orchid, palm, reed) prevent mechanical failure through a combination of initiation of growth with a stem that is sufficiently wide for future supply and support demands, and an increase in the stem diameter and strength by cell wall expansion and lignification. Some monocot plants attain tree stature comparable to that of arborescent dicotyledons and conifers (*e.g.* palm trees with maximum heights of 20-40 meters), but their stems are relatively slender [21]. By contrast, tall dicot trees have bigger stem diameters relative to their height than small trees. (The opposite behaviours of dicot and monocot stems also inspired La Fontaine's fable "The oak and the reed", and the intriguing story was illustrated in a painting by A.E. Michallon, now at Fitzwilliam Museum). Although the wood density representing the relative quantity of the cell wall in a given volume of wood tissue vary significantly among wood species, the composition and strength of the cell wall is generally the same for all woods [1, 7]. Bone tissue is another example of natural cellular structure where apposition and resorption of cellular matter is controlled by the magnitude of the stresses, with bones becoming denser at the point of stress [24, 26].

For living cellular structures, there are many physiological and ecological factors that affect their mechanical properties, and they also change over time [2,18]. Nevertheless, for structures with uniform cell size, wall thickness, and shape, the fundamental question arises *whether the same volume of cell wall material has the same effect when arranged as many small cells or as fewer large cells* (see Figure 1). To answer this question, in the case of small strain elastic deformations, thresholds on stiffness or strength can be set as constraints in the mechanical design or when modelling developmental processes [9, 10]. However, if large strains occur during functional or physiological changes, then finding suitable criteria to account for the nonlinear elastic properties of the deforming cell walls is more challenging [15, 16].

*School of Mathematics, Cardiff University, Senghennydd Road, Cardiff, CF24 4AG, UK, Email: MihaiLA@cardiff.ac.uk

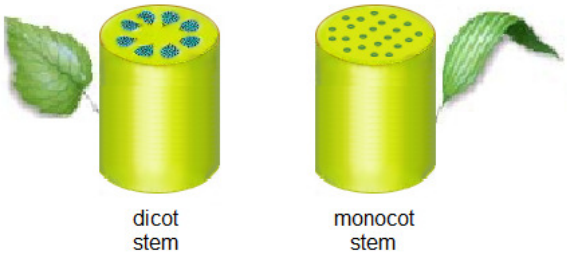

Figure 1: Schematic of dicotyledon and monocotyledon stems.

In this study, for cellular bodies of nonlinear elastic material [19, 25], we investigate numerically the utility of a nonlinear parameter which correlates with the softness and the load-bearing capacity of these structures, and explore a possible approach for their optimisation process. For finite element models of periodic structures of Mooney-type material with different structural geometry and subject to large strain deformations, we identify a nonlinear elastic modulus as the ratio between the mean effective stress and the mean effective strain in the solid cell walls, and show that this modulus increases when the thickness of the walls increases, as well as when the number of cells increases while the volume of solid material remains fixed. Since, under the specified conditions, this nonlinear elastic modulus increases also as the corresponding mean stress increases, either the mean modulus or the mean stress can be employed as indicator when the optimum wall thickness or number of cells is sought. Cellular structures are typically difficult to optimize due to the complex interaction between the geometry and the nonlinear properties of the constitutive material, and finding a nonlinear parameter that is monotonic would guarantee at least that the set of acceptable values is non-empty.

Furthermore, while for cellular structures of linearly elastic material, the mean elastic modulus is known to increase when the ratio between the thickness and the length of the cell wall increases [9,10], our results show that, for structure made from a nonlinear hyperelastic material, this elastic modulus increases also when the cell size decreases while both the total material volume and the ratio between the thickness and the length of the cell walls remain fixed. While different factors may contribute to this behaviour, in our view, this increase in the elastic modulus is due to the enhanced elasticity of the cell walls when more material is added or when the same elastic material is distributed more uniformly throughout the structure. This type of elastic responses was also observed when the cells were filled with an elastic core, as demonstrated by Mihai *et al.* [17], and the elasticity of the deforming walls was further augmented by the contact with the cell core.

Cellular materials are the subject of intensive research efforts in biomedical applications, where the advent of 3D printing has led to increased interest in the optimal design of tissue scaffolds with controlled, reproducible geometries. Engineered tissue scaffolds provide an environment for biological cells to grow and regenerate tissue, and their composition, micro-structure and mechanical properties play a critical role in the response of biological cells that migrate within them. In highly oriented tissues, such as nerve, ligament, muscle, and tendon, where tensile strength and stiffness are controlled by collagen fibers, geometrically well-defined scaffolds also provide guidance cues for cells and fibers orientation [5, 13, 22]. For these type of structures, the cell density and wall stiffness are key factors [4, 6, 23, 28], which can be independently optimized to improve biological response [3, 8, 27].

2 Periodic cellular structures

In this section, we assess computationally nonlinear elastic deformation effects in periodic cellular structures of hyperelastic material by defining a nonlinear parameter and then testing its monotonicity with respect to the wall thickness as well as to the number of cells when the material volume is fixed. To test the independent influence of mechanical features, such as the cell size and the number of cells, on the collective behaviour of a group of cells under large strain deformations, we model periodic, honeycomb-like structures with regular geometry, such as square, diamond-shape, and hexagonal cells.

The computer models analysed here are formed from a single piece of elastic material which occupies a thin square domain of (dimensionless) side one in the X-(horizontal) and Y-(vertical) directions, and 0.1 in the Z-(out-of-plane) direction, and the cells are equal in size throughout the structure. Each structure is deformed by imposing the following boundary conditions: the lower external horizontal face is fixed in the second/vertical/Y-direction and free to slide in the first/horizontal/X-direction and in the third/out-of-plane/Z-direction; the upper external horizontal face is subject to a prescribed vertical stretch of 50% and is free to slide horizontally and out-of-plane; and the remaining external and internal cell faces deform freely. The numerical results recorded here were obtained by a standard finite element procedure implemented within the Finite Elements for Biomechanics (FEBio) software environment [14]. The model structures were created in SolidWorks and imported into the FEBio software, and a mesh refinement study was performed for each structure, so that the numerical results are independent of the mesh-size.

For a homogeneous isotropic incompressible elastic wall described by a strain energy density function $\mathcal{W}(I_1, I_2, I_3)$ and subject to finite elastic deformations, the Cauchy stress takes the form: $\boldsymbol{\sigma} = -p\mathbf{I} + \beta_1\mathbf{B} + \beta_{-1}\mathbf{B}^{-1}$, where $\mathbf{B}$ is the left Cauchy-Green strain tensor, I_1, I_2, I_3 are the principal strain invariants, $\beta_1 = 2\partial\mathcal{W}/\partial I_1$, $\beta_{-1} = -2\partial\mathcal{W}/\partial I_2$ are the material response coefficients, and p is the arbitrary hydrostatic pressure [19,25]. For the cell wall material, two different hyperelastic models were chosen, as follows.

(NH) The generalised neo-Hookean model characterised by the strain energy density function:

$$\mathcal{W}(I_1, I_2, I_3) \;=\; \frac{\mu}{2}\left(I_1 - 3 - \ln I_3\right) + \frac{\lambda}{2}\left(\ln I_3^{1/2}\right)^2, \tag{2.1}$$

where $\mu = E/[2(1+\nu)] > 0$ and $\lambda = \nu E/[(1+\nu)(1-2\nu)] > 0$ are constant parameters. In the computed examples, we set $E = 0.1$ MPa and $\nu = 0.49$.

(MR) The generalised Mooney-Rivlin model described by the strain energy density function:

$$\mathcal{W}(I_1, I_2, I_3) \;=\; \frac{\mu_1}{2}\left(I_3^{-1/3} I_1 - 3\right) + \frac{\mu_2}{2}\left(I_3^{-2/3} I_2 - 3\right) + \frac{\kappa}{2}\left(I_3^{1/2} - 1\right)^2, \tag{2.2}$$

where μ_1, μ_2, κ are constants, such that $\mu = \mu_1 + \mu_2 > 0$ and $\kappa > 0$. In the numerical models, we set $\mu_1 = 0.0016$ MPa, $\mu_2 = 0.032$ MPa, $\kappa = 1.6667$ MPa.

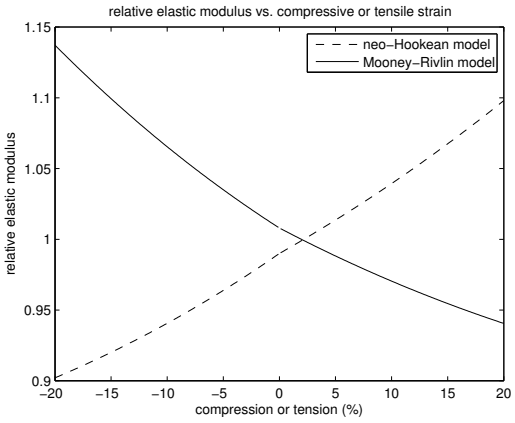

Figure 2: Nonlinear elastic modulus $\mathcal{E}$ normalised to E for the NH and MR models.

These models were selected for their different mechanical behaviours under finite tension or compression. Specifically, setting the nonlinear elastic modulus as the ratio between the Cauchy stress and the logarithmic strain in the direction of the applied tensile or compressive force:

$$\mathcal{E} = \frac{a^3 - 1}{a^2 \ln a}\left(a\beta_1 - \beta_{-1}\right), \tag{2.3}$$

where $a > 0$ is the stretch in the corresponding direction, for the NH material (2.1), this modulus increases under increasing tension and decreases under increasing compression, while for the MR

material (2.2), the modulus (2.3) decreases with the increasing tension and increases with the increasing compression (see Figure 2).

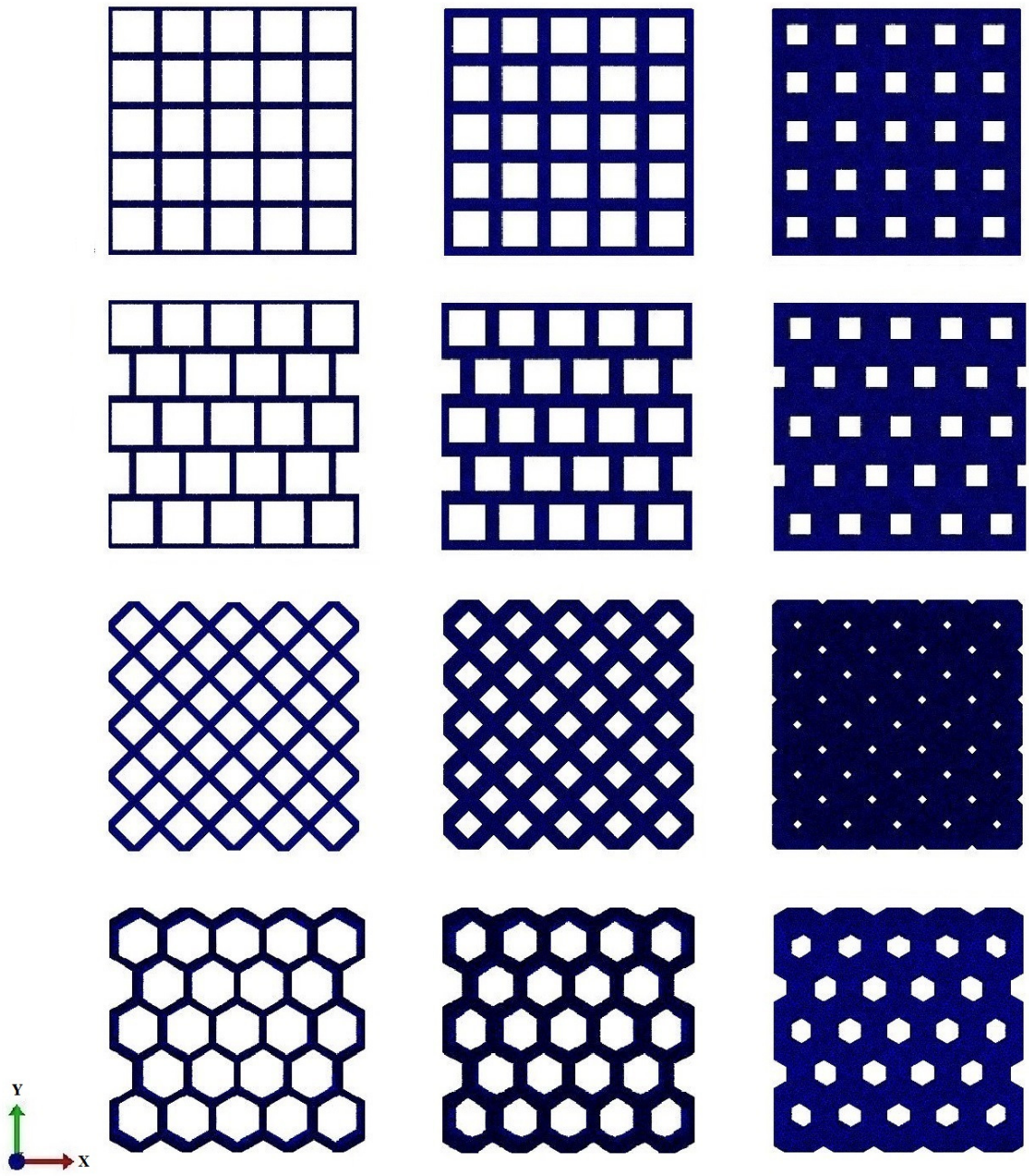

Figure 3: Undeformed model structures with stacked (top row), staggered (middle top row), diamond (middle bottom row), and hexagon (bottom row) cell geometry, and thin (left column), medium (middle column), and thick (right column) cell walls.

The undeformed structures with uniform cell size and different wall thickness are represented in Figure 3. In Figure 4, the deformed structures of NH material are shown. Note that the initially horizontal walls of the staggered cells bend and the inclined walls of the diamond and hexagon cells are sheared. Similar deformations were observed in structures of MR material. For the model structures, the mean values of the effective Cauchy stress *vs.* those of the effective logarithmic strain $\ln \mathbf{B}^{1/2} = \ln \sqrt{2\mathbf{E}+1}$, where $\mathbf{B}$ is the left Cauchy-Green strain tensor, $\mathbf{E}$ is the corresponding Green-Lagrange strain tensor, and the logarithmic function is applied component-wise, are indicated in Figures 5-8 (a,

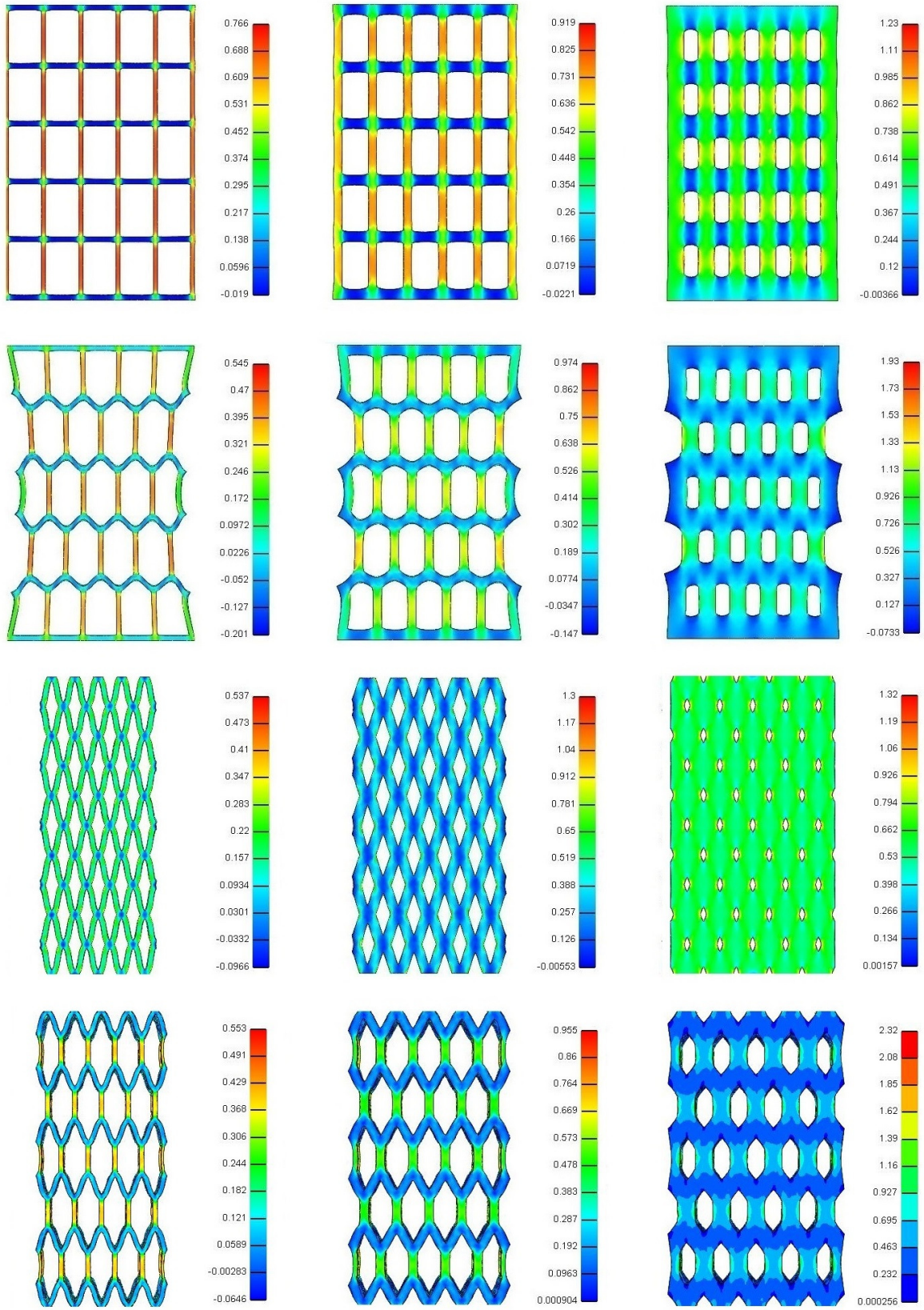

Figure 4: Deformed structures with stacked (top row), staggered (middle top row), diamond (middle bottom row), and hexagon (bottom row) cell geometry, and thin (left column), medium (middle column), and thick (right column) cell walls of NH material subject to 50% stretch in the vertical direction, showing the non-homogeneous Green-Lagrange strains in the same direction.

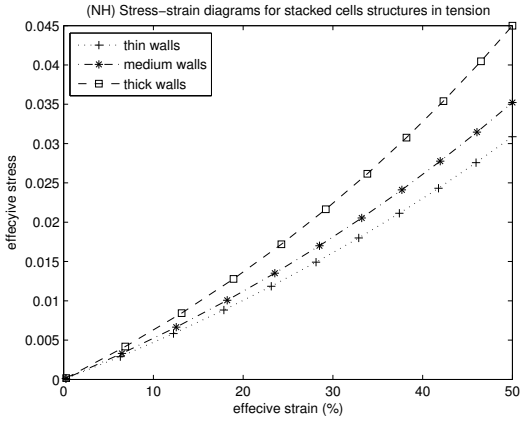

(a)

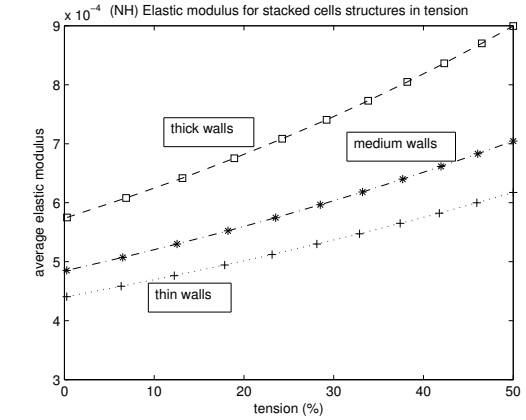

(b)

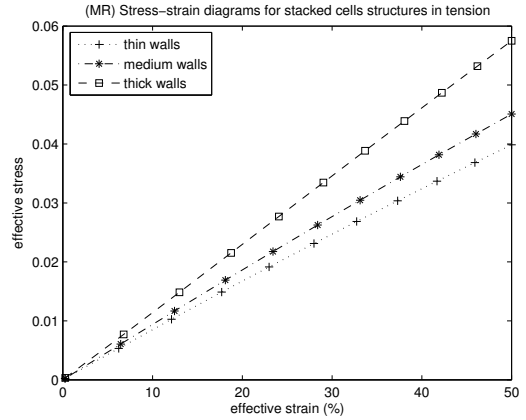

(c)

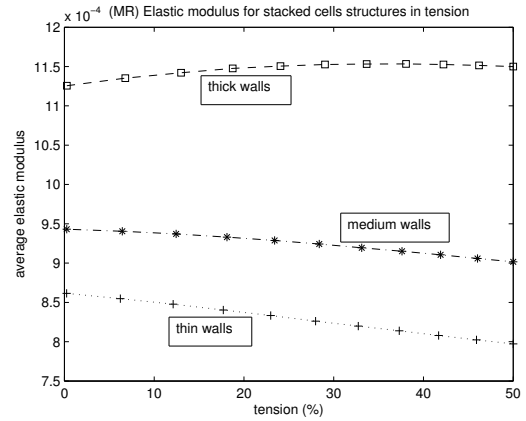

(d)

Figure 5: (a,c) Mean effective Cauchy stress (MPa) and (b,d) nonlinear elastic modulus (MPa) *vs.* mean effective logarithmic strain for stacked cells structures of (a,b) NH and (c,d) MR material with different wall thickness.

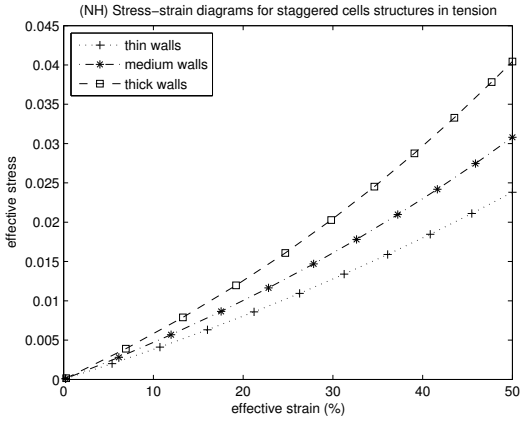

(a)

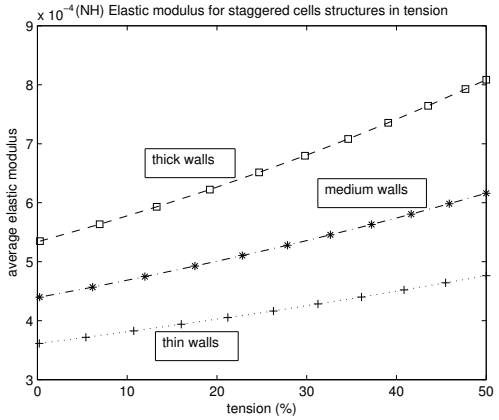

(b)

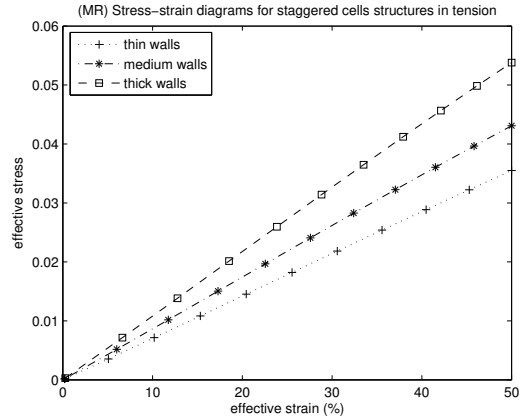

(c)

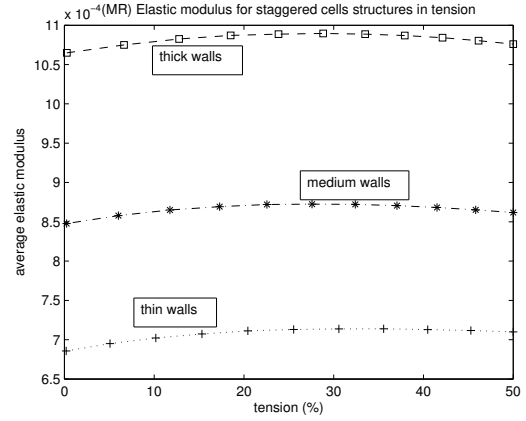

(d)

Figure 6: (a,c) Mean effective Cauchy stress (MPa) and (b,d) nonlinear elastic modulus (MPa) *vs.* mean effective logarithmic strain for staggered cells of (a,b) NH and (c,d) MR material with different wall thickness.

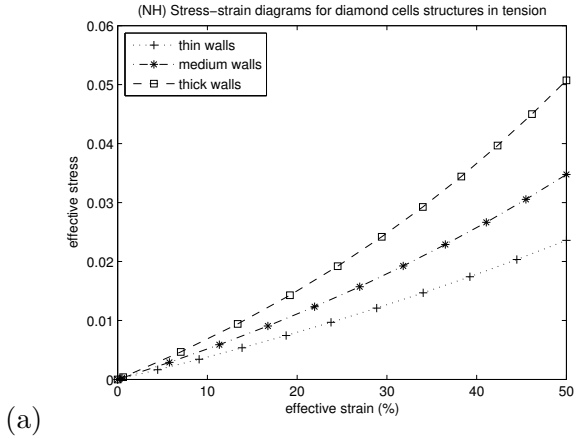

(a)

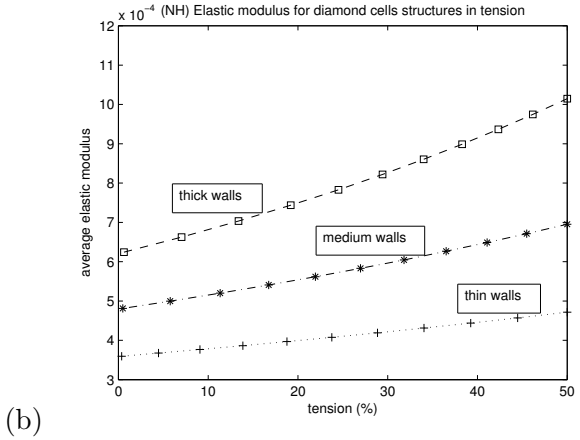

(b)

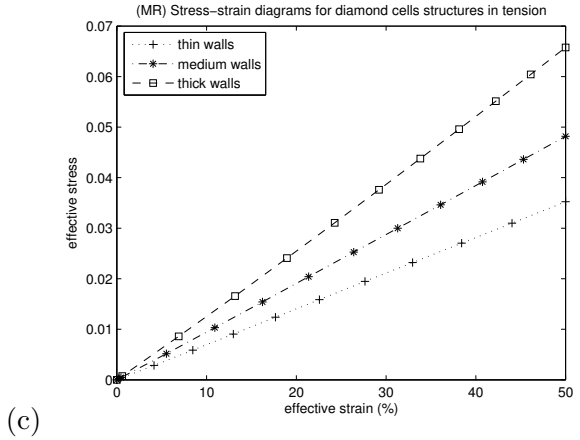

(c)

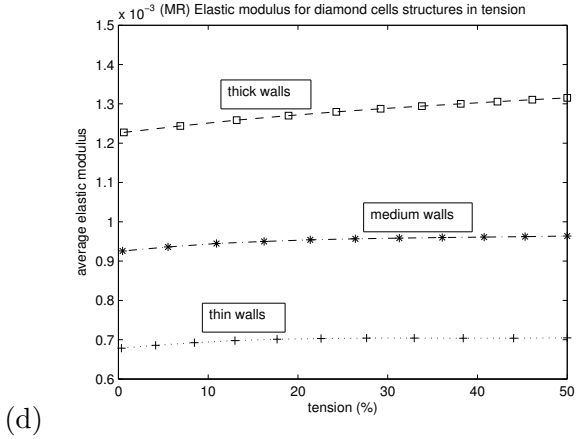

(d)

Figure 7: (a,c) Mean effective Cauchy stress (MPa) and (b,d) nonlinear elastic modulus (MPa) *vs.* mean effective logarithmic strain for diamond cells of (a,b) NH and (c,d) MR material with different wall thickness.

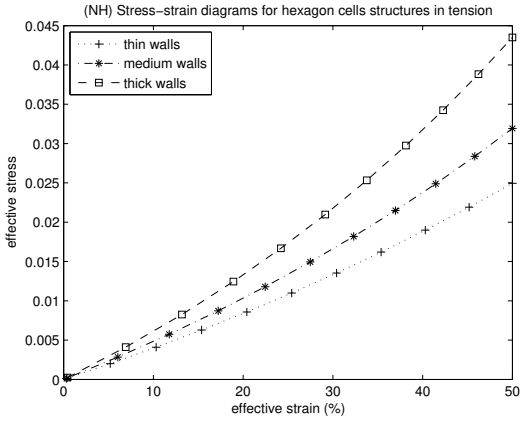

(a)

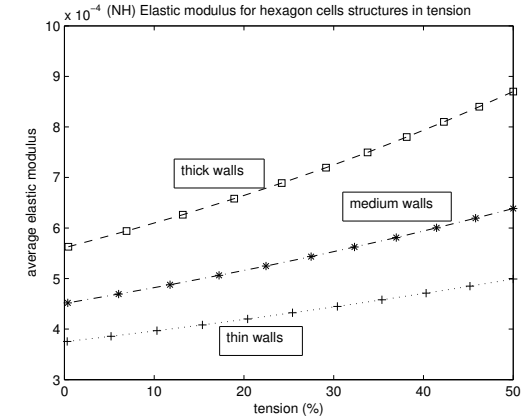

(b)

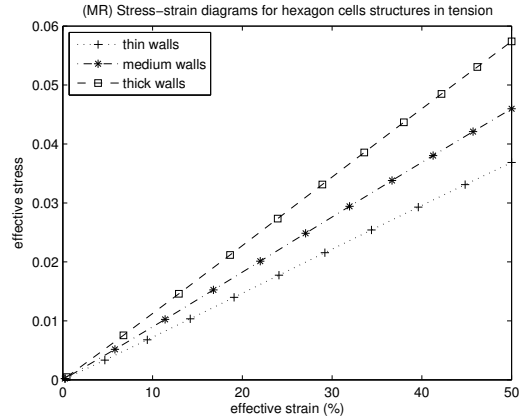

(c)

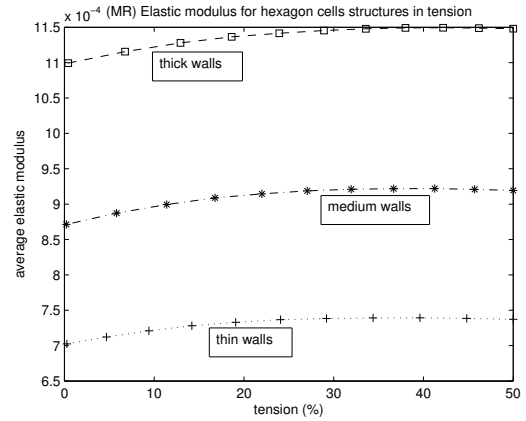

(d)

Figure 8: (a,c) Mean effective Cauchy stress (MPa) and (b,d) nonlinear elastic modulus (MPa) *vs.* mean effective logarithmic strain for hexagon cells of (a,b) NH and (c,d) MR material with different wall thickness.

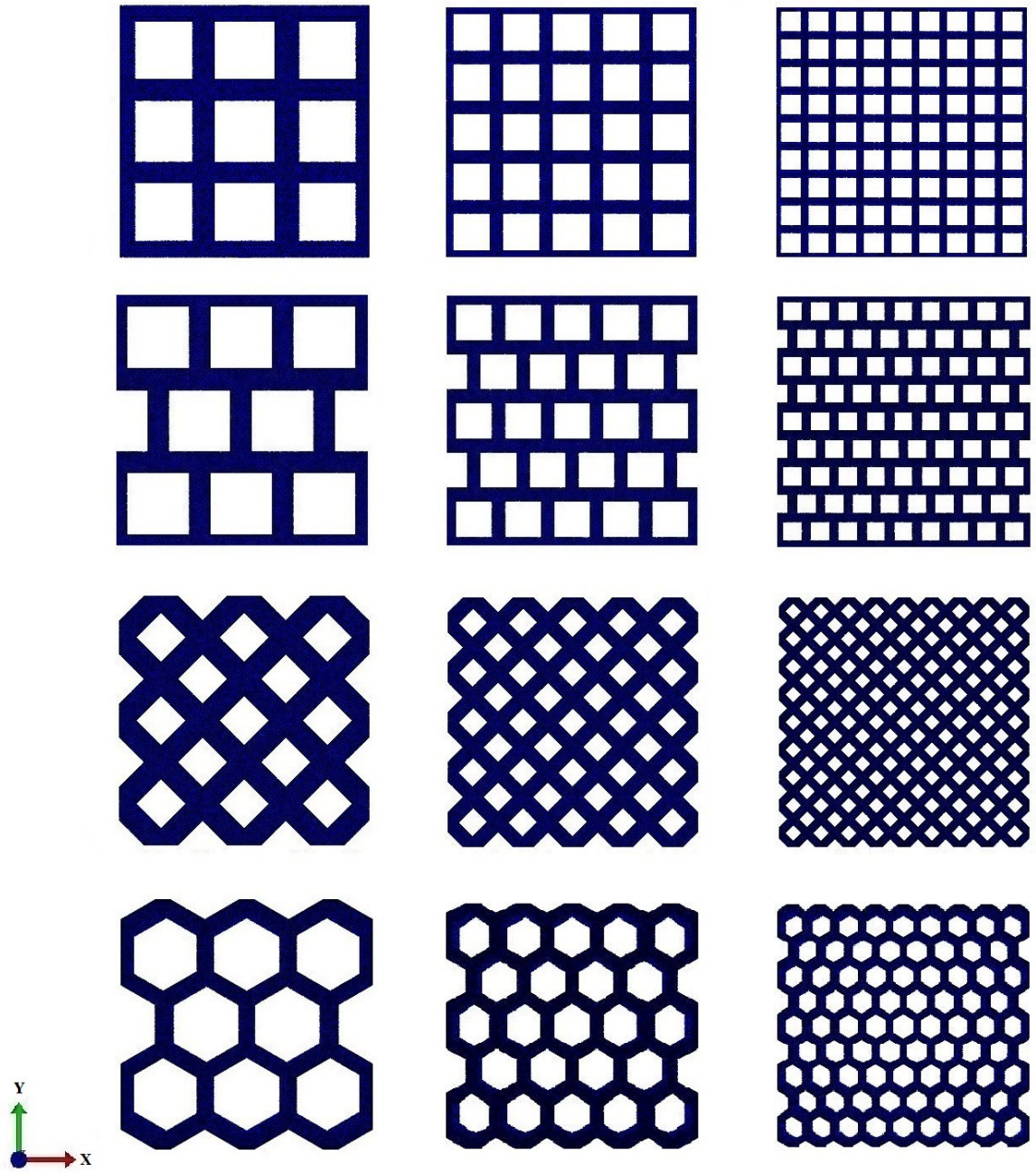

Figure 9: Undeformed model structures with stacked (top row), staggered (middle top row), diamond (middle bottom row), and hexagon (bottom row) cell geometry, and 3×3 (left column), 5×5 (middle column), and 9×9 (right column) cells.

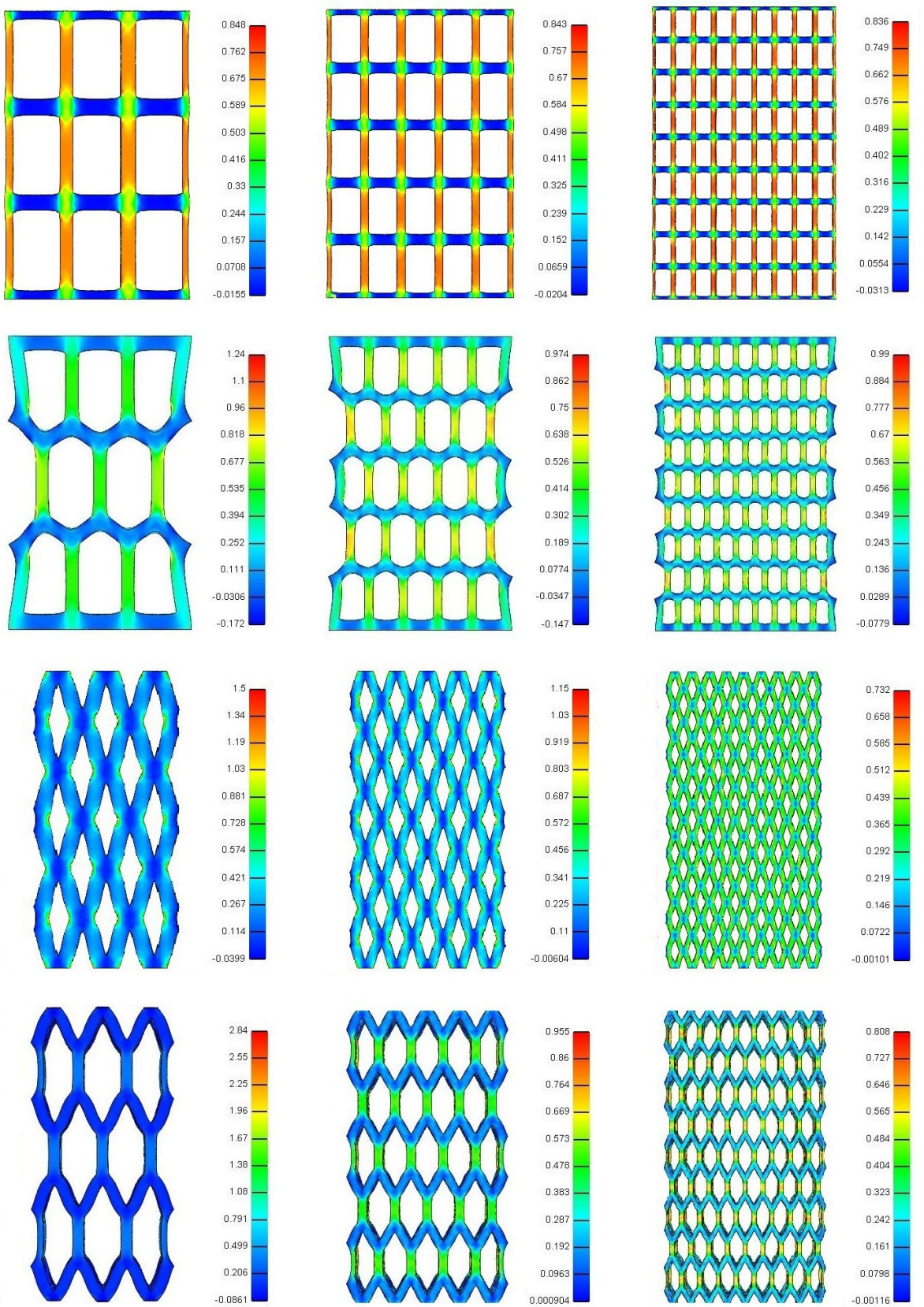

Figure 10: Deformed structures with stacked (top row), staggered (middle top row), diamond (middle bottom row), and hexagon (bottom row) cell geometry, and 3×3 (left column), 5×5 (middle column), and 9×9 (right column) cells of NH material subject to 50% stretch in the vertical direction, showing the non-homogeneous Green-Lagrange strains in the same direction.

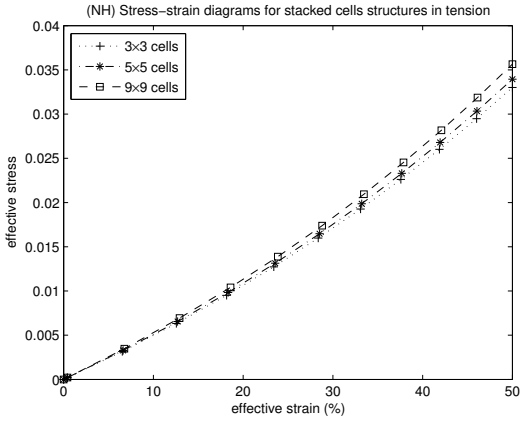

(a)

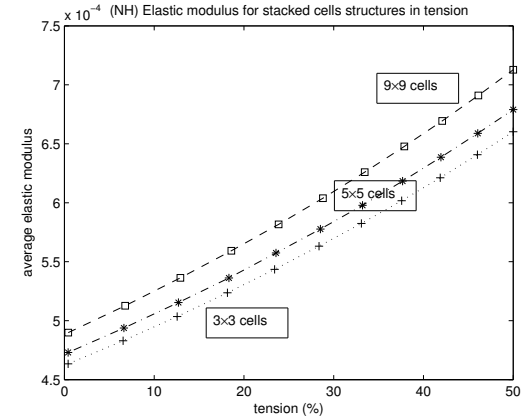

(b)

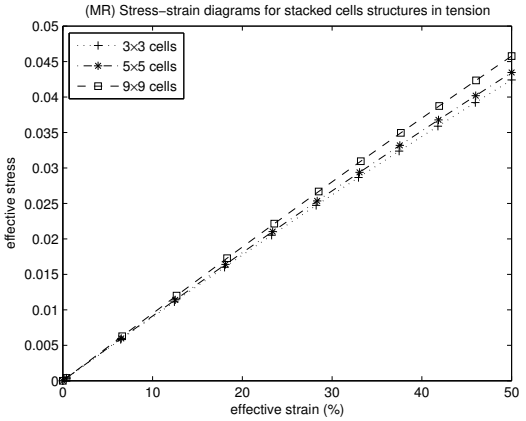

(c)

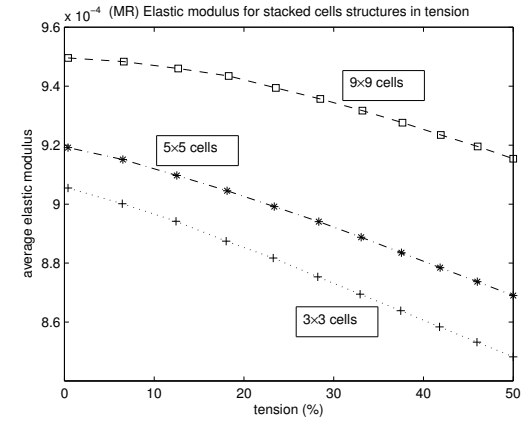

(d)

Figure 11: (a,c) Mean effective Cauchy stress (MPa) and (b,d) nonlinear elastic modulus (MPa) *vs.* mean effective logarithmic strain for stacked cells of (a,b) NH and (c,d) MR material with different number of cells and fixed material volume.

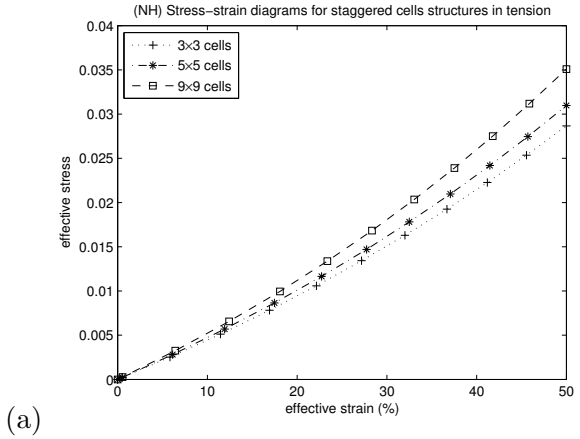

(a)

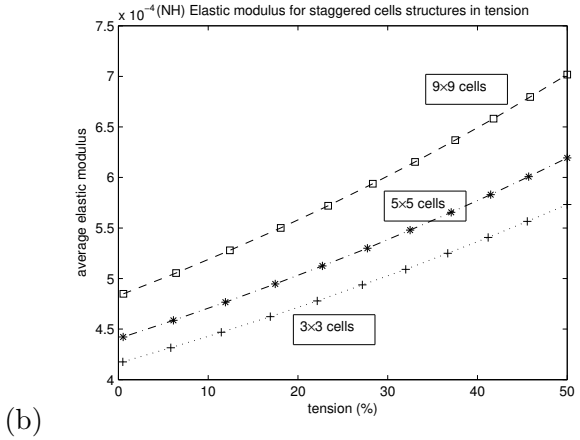

(b)

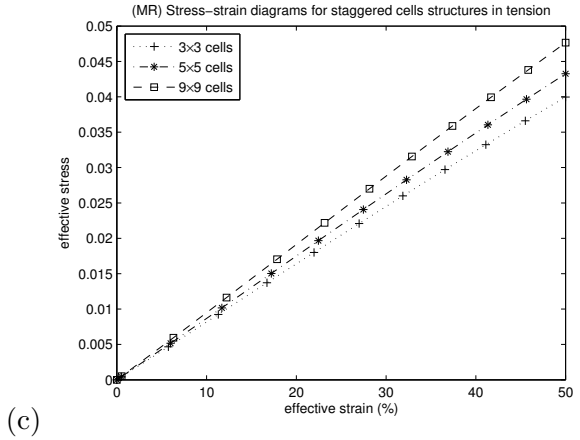

(c)

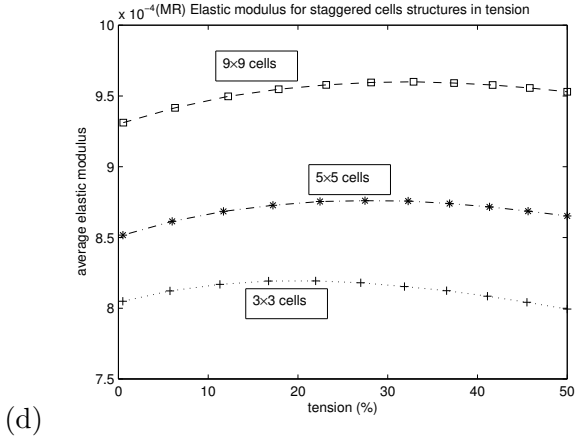

(d)

Figure 12: (a,c) Mean effective Cauchy stress (MPa) and (b,d) noninear elastic modulus (MPa) *vs.* mean effective logarithmic strain for staggered cells of (a,b) NH and (c,d) MR material with different number of cells and fixed material volume.

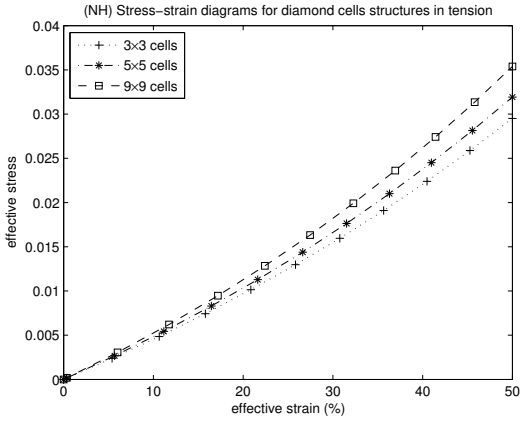

(a)

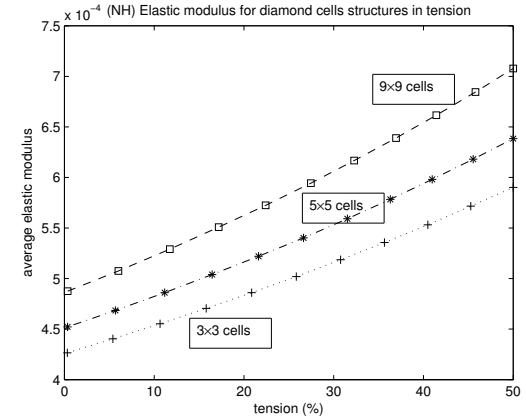

(b)

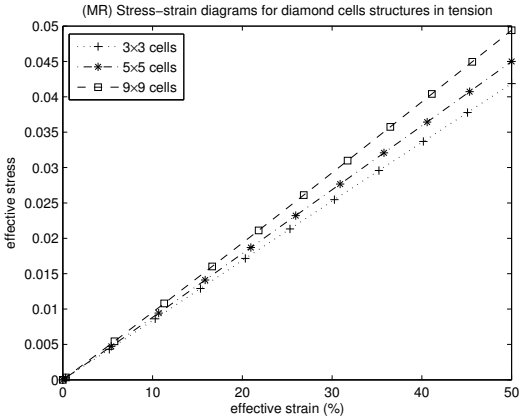

(c)

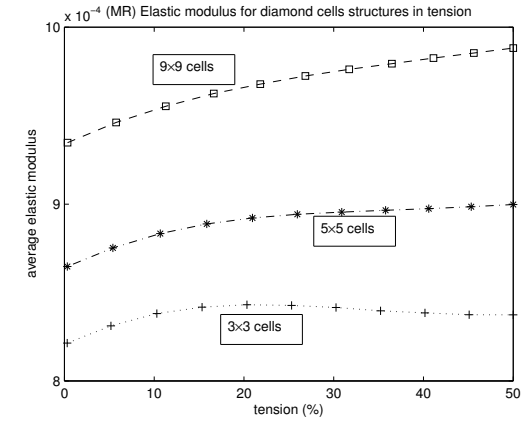

(d)

Figure 13: (a,c) Mean effective Cauchy stress (MPa) and (b,d) nonlinear elastic modulus (MPa) *vs.* mean effective logarithmic strain for diamond cells of (a,b) NH and (c,d) MR material and with different number of cells and fixed material volume.

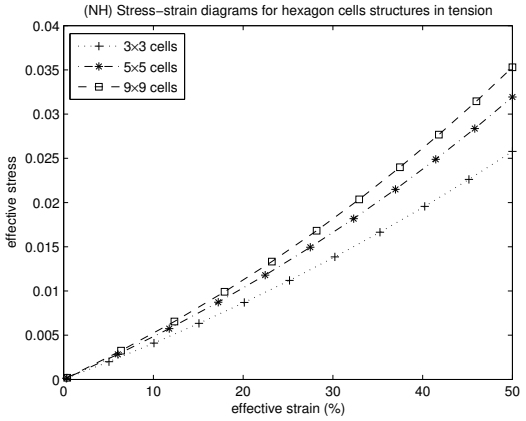

(a)

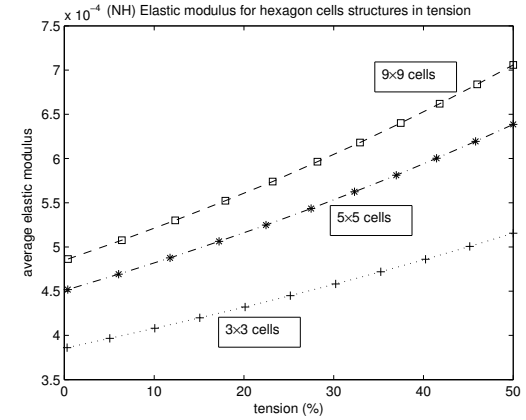

(b)

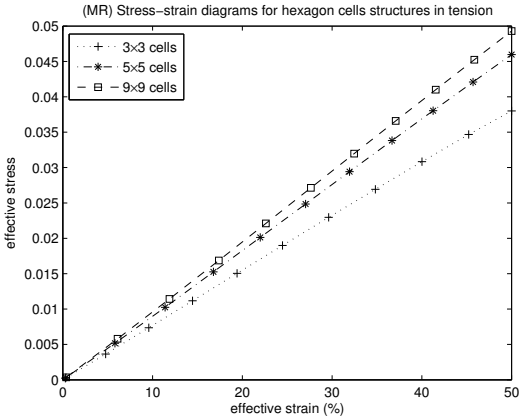

(c)

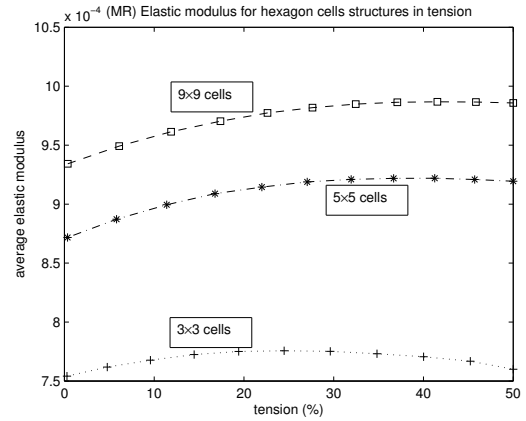

(d)

Figure 14: (a,c) Mean effective Cauchy stress (MPa) and (b,d) nonlinear elastic modulus (MPa) *vs.* mean effective logarithmic strain for hexagon cells of (a,b) NH and (c,d) MR material and with different number of cells and fixed material volume.

c). We recall that the effective value of a symmetric tensor $\mathbf{s}$ is defined as [11, 12]

$$\begin{aligned} s_{\text{eff}} &= \sqrt{\frac{3}{2}\left[\left(\mathbf{s}-\frac{1}{3}\text{tr}(\mathbf{s})\mathbf{I}\right):\left(\mathbf{s}-\frac{1}{3}\text{tr}(\mathbf{s})\mathbf{I}\right)\right]} \\ &= \sqrt{s_{11}^2+s_{22}^2+s_{33}^2-s_{11}s_{22}-s_{22}s_{33}-s_{33}s_{11}+3\left(s_{12}^2+s_{13}^2+s_{23}^2\right)}. \end{aligned} \tag{2.4}$$

The mean value was calculated as the sum of the values on all the finite elements divided by the number of elements. The values of the associated *nonlinear elastic modulus* defined as the ratio between the mean effective Cauchy stress and the mean effective logarithmic strain are represented in Figures 5-8 (b, d), respectively. The numerical results suggest that both the stress and the elastic modulus increase with the cell wall thickness.

In Figure 9, the undeformed structures with uniform cell size and an increasing number of cells while the volume of solid material remains unchanged are illustrated. In these models, for the stacked and diamond cells, the ratio between the thickness and the length of the cell walls is also unchanged as the number of cells increases, while for the staggered and hexagonal cells, this ratio increases slightly. The deformed structures of NH material are shown in Figure 10. For the structures with an increasing number of cells, the mean values of the effective Cauchy stress *vs.* those of the effective logarithmic strain are recorded in Figures 11-14 (a, c). The corresponding values of the *mean elastic modulus* are indicated in Figures 11-14 (b, d). These results show that both the stress and the mean elastic modulus increase as the number of cells increases while the volume of material remains unchanged.

The results obtained for the structures with increasing wall thickness and with an increasing number of cells imply that, for cellular structures with similar cell geometries, if the number of cells increases while the wall thickness is fixed, then the mean elastic modulus in the walls increases with the number of cells. This result is consistent with the classical result that the mean elastic modulus in a cellular structure increases as the ratio between the thickness and the length of the cell walls increases. However, for cellular structures of nonlinear elastic material, the elastic modulus may also increase if the ratio between the thickness and the length of the cell walls is fixed while the cell size decreases and the total material volume remains unchanged, as shown by our computer models with stacked and diamond cells.

3 Optimisation problem

Due to its monotonic behaviour, the nonlinear mean elastic modulus investigated above can be employed to determine the minimum wall thickness or the number of cells under the corresponding deformations by formulating the following optimisation problem:

$$\text{find } d_0 = \min_{d\in V} d, \quad V = \left\{ d > 0 \;\middle|\; \bar{\mathcal{E}}(d) \geq C \right\},$$

where d is the wall thickness or the number of cells, $\bar{\mathcal{E}}$ is the mean elastic modulus for the chosen deformation and under the given boundary conditions, and $C > 0$ is the given target value.

Equivalently, the objective d_0 may be characterised as follows:

$$\text{find } d_0 = \min\left\{ d \mid V \neq \emptyset \right\}.$$

Since $\bar{\mathcal{E}}$ is an increasing function of its argument, the range of admissible values V is a non-empty set, and hence the existence of a solution to the optimisation problem is guaranteed. The epigraph of the associated optimisation function is illustrated graphically in Figure 15.

Cellular structures of nonlinear elastic material are difficult to optimise due to the complex interaction between the geometry and the nonlinear properties of the cell wall material, and finding a nonlinear parameter that is monotonic will guarantee at least that the feasibility constraints are met, and hence the set of feasible values is non-empty. Since, under the specified conditions, the mean elastic modulus increases as the corresponding mean stress increases, either the mean stress or the mean modulus can be used as indicator when the optimum wall thickness or number of cells is sought.

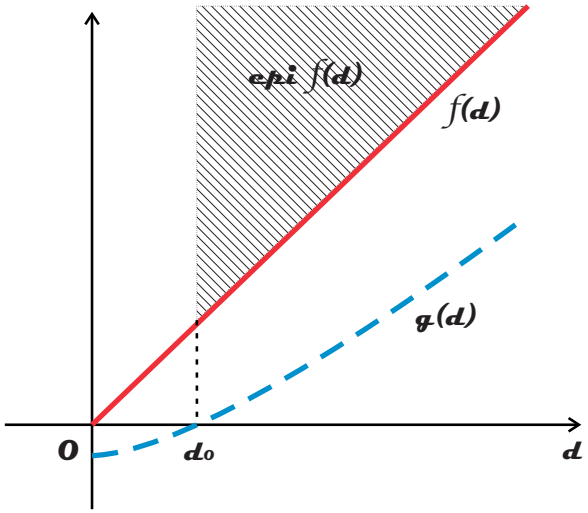

Figure 15: Epigraph of function $f : V = \{d > 0 \mid g(d) \geq 0\} \to \mathbb{R},\ f(d) = d,\ g(d) = \bar{\mathcal{E}}(d) - C$.

4 Conclusion

Cellular bodies are strong, pliable structures made from seemingly fragile materials. Among the best known mechanical qualities of these structures are their high strength-to-weight ratio and energy absorption capacity, which arise from the inextricable relation between the geometric architecture and the nonlinear elastic responses of their constituents. In many natural and engineered cellular materials, during functional performance, plastic damage or fracture rarely occurs, and the material recovers completely after large deformations. Such deformations can be reasonably treated within the theoretical framework of large strain elasticity, which in principle provides a complete description of the elastic responses of a solid material under loading.

In this paper, for cellular structures of nonlinear hyperelastic material with uniform cell size, wall thickness, and shape, we showed that the same volume of material leads to different mechanical behaviours when arranged as many small cells than when organised as fewer large cells, and explored a possible approach that could be useful in their optimisation process. This approach consists in identifying a nonlinear parameter which, under certain restrictions (material, geometric, and external conditions), is monotonic with respect to the wall thickness or the number of walls, and may be useful as indicator when the optimum wall thickness of number of cells is sought (for example, in soft tissue scaffolds, where the cell density and the wall stiffness play critical roles in their performance). Far from claiming the universality of this nonlinear parameter, the general approach developed here may illuminate certain mechanical behaviour of cellular structures of nonlinear elastic material, which are typically difficult to optimize.

References

[1] Ashby MF, Easterling KE, Harrysson R, Maiti SK. 1985. The fracture and toughness of woods, Proceedings of the Royal Society A 398, 261-280.

[2] Bassel GW, Stamm P, Mosca G, de Reuille PB, Gibbs DJ, Winter R, Janka A, Holdsworth MJ, Smith RS. 2014. Mechanical constraints imposed by 3D cellular geometry and arrangement modulate growth patterns in the Arabidopsis embryo, Proceedings of the National Academy of Sciences 111, 8685-8690.

[3] Boccaccio A, Uva AE, Fiorentino M, Lamberti L, Monno G. 2016. A mechanobiology-based algorithm to optimize the microstructure geometry of bone tissue scaffolds, International Journal of Biological Sciences 12, 1-17.

[4] Discher DE, Janmey P, Wang Y. 2005. Tissue cells feel and respond to the stiffness of their substrate, Science 310, 1139-1143.

[5] Engelmayr Jr. GC, Papworth GD, Watkins SC, Mayer Jr. JE, Sacks MS. 2006. Guidance of engineered tissue collagen orientation by large-scale scaffold microstructures, Journal of Biomechanics 39, 1819-1831.

[6] Engler AJ, Sen S, Lee Sweeney H, Discher DE. 2006. Matrix elasticity directs stem cell lineage specification, Cell 126, 677-689.

[7] Fournier M, Dlouhá J, Jaouen G, Almeras T. 2013. Integrative biomechanics for tree ecology: beyond wood density and strength, Journal of Experimental Botany, doi:10.1093/jxb/ert279.

[8] Gariboldi MI, Best SM. 2015. Effect of ceramic scaffold architectural parameters on biological response, Frontiers in Bioengineering and Biotechnology, doi: 10.3389/fbioe.2015.00151.

[9] Gibson LJ, Ashby MF. 1997. Cellular Solids: Structure and Properties, 2nd ed, Cambridge University Press.

[10] Gibson LJ, Ashby MF, Harley BA. 2010. Cellular Materials in Nature and Medicine, Cambridge University Press.

[11] Hutchinson JW, Neale KW. 1981. Finite strain J_2 deformation theory, Proceeding of the IUTAM Symposium on Finite Elasticity, Martinus Nijhoff Publishers, Netherlands.

[12] Jung D, Gea HC. 2004. Topology optimization of nonlinear structures, Finite Elements in Analysis and Design 40, 1417-1427.

[13] Knychala J, Bouropoulos N, Catt CJ, Katsamenis OL, Please CP, Sengers BG. 2013. Pore geometry regulates early stage human bone marrow cell tissue formation and organisation, Annals of Biomedical Engineering 41, 917-930.

[14] Maas SA, Ellis BJ, Ateshian GA, Weiss J. 2012. FEBio: Finite Elements for Biomechanics, Journal of Biomechanical Engineering 134.

[15] Mihai LA, Goriely A. 2014. Nonlinear Poisson effects in soft honeycombs, Proceedings of the Royal Society A 470, 20140363.

[16] Mihai LA, Goriely A. 2015. Finite deformation effects in cellular structures with hyperelastic cell walls, International Journal of Solids and Structures 53, 107-128.

[17] Mihai LA, Alayyash K, Goriely A. 2015. Paws, pads, and plants: The enhanced elasticity of cell-filled load-bearing structures, Proceedings of the Royal Society A 471, 20150107.

[18] Niklas KJ. 1992. Plant Biomechanics: An Engineering Approach to Plant Form and Function, Chicago, IL, University of Chicago Press.

[19] Ogden RW. 1997. Non-Linear Elastic Deformations, 2nd ed, Dover, New-York.

[20] Pauwels F. 1980. Biomechanics of the locomotor apparatus: contributions on the functional anatomy of the locomotor apparatus, Springer, Berlin.

[21] Rich PM. 1986. Mechanical architecture of arborescent rain forest palms, Principes 30, 117-131.

[22] Rumpler M, Woesz A, Dunlop JW, van Dongen JT, Fratzl P. 2008. The effect of geometry on three-dimensional tissue growth, Journal of thr Royal Society Interface 5, 1173-1180.

[23] Shih YRV, Tseng KF, Lai HY, Lin CH, Lee, OK. 2011. Matrix stiffness regulation of integrin-mediated mechanotransduction during osteogenic differentiation of human mesenchymal stem cells, Journal of Bone and Mineral Research 26, 730-738.

[24] Taylor MP, Wedel MJ. 2013. Why sauropods had long necks; and why giraffes have short necks, PeerJ 1, 1-41, doi:10.7717/peerj.36.

[25] Truesdell C, Noll W. 2004. The Non-Linear Field Theories of Mechanics, Springer-Verlag, New York, 3rd ed.

[26] van Schalkwyk OL, Skinner JD, Mitchell G. 2004. A comparison of the bone density and orphology of giraffe (Giraffa camelopardalis) and buffalo (Syncerus caffer) skeletons, Journal of Zoology: Proceedings of the Zoological Society of London 264, 307-315.

[27] Wieding J, Wolf A, Bader R. 2014. Numerical optimization of open-porous bone scaffold structures to match the elastic properties of human cortical bone, Journal of the Mechanical Behavior of Biomedical Materials 37, 56-68.

[28] Zhang H, Landmann F, Zahreddine H, Rodriguez D, Koch M, Labouesse M. 2011. A tension-induced mechanotransduction pathway promotes epithelial morphogenesis, Nature 471, 99-103.